Seventh International Conference on CFD in the Minerals and Process Industries
CSIRO, Melbourne, Australia
9-11 December 2009

GRID CONVERGENCE STUDY FOR A TWO-DIMENSIONAL SIMULATION OF FLOW AROUND A SQUARE CYLINDER AT A LOW REYNOLDS NUMBER

Mohamed Sukri Mat ALI[♦] , Con J. DOOLAN[♦] and Vincent WHEATLEY[♣]

[♦]School of Mechanical Engineering, The University of Adelaide, South Australia 5005, AUSTRALIA
[♣]School of Engineering, The University of Queensland, Queensland 4072, AUSTRALIA

ABSTRACT

This paper describes a systematic method of refining a computational grid for the Direct Numerical Simulation (DNS) of flow about a square cylinder. The grid refinement method involves two stages. The first stage constructs computational meshes based on reasonable estimates of cell size and grid stretching ratios and investigates the sensitivity of the computed flow field to these parameters. The findings from this stage are used as a guide for further grid refinement. In the second stage, the grid is divided into four regions to minimise the grid stretching ratio. The smallest cell is sized so the boundary layer on the front face of the cylinder is adequately resolved. Solutions on seven different grids are presented to investigate the effect of numerical scheme, boundary conditions and grid independence. The level of grid independence is evaluated using a form of Richardson extrapolation and the study shows that the finest grid solution has a Grid Convergence Index (GCI) of less than 5%.

INTRODUCTION

The study of flow around a square cylinder has been and continues to be the subject of intense research (Sohankar *et al.*; 1998, Saha *et al.*;2002, Ozgoren;2005, Inoue *et al.*; 2006 and Doolan;2009). Owing to its simplicity, this shape has become important for the study of the fundamental properties of bluff body wakes. These types of wakes are almost ubiquitous in all fields of engineering. For example, many types of flow mixers rely on bluff body wakes to enhance mixing.

Within the scope of predicting the flow field around a square cylinder using numerical analysis, many similar investigations have been made, but the results always show small discrepancies even though the overall global trends are similar. One of the reasons for these discrepancies is the difference in the construction of the mesh. Sohankar *et al.* (1998) for example, constructed a non-uniform mesh near the wall of a square cylinder and, at 5 diameters away from the cylinder surface, a uniform mesh was applied. The size of the smallest cell was located at the leading edge of the square cylinder with cell size of $h/D = 0.004$. Another similar study was carried out by Inoue *et al.* (2006). They constructed a non-uniform mesh but divided the computational domain into three regions, each with a different grid ratio. The smallest cell was located along the edges of the square cylinder with the value of $h/D = 0.01$. The most recent study by Doolan (2009) investigated the grid convergence for three different grid resolutions on DNS around a square cylinder and found that the solution converged when the smallest cell size along the square cylinder edge was $h/D = 0.0167$.

The DNS results from the three examples show similar physical flow features, such as vortex shedding, but there are small discrepancies in the integrated variables e.g., Strouhal number (St), root mean square lift coefficient (CL_{rms}) and mean drag coefficient (CD_{mean}). It is well accepted by the CFD community that the error from the numerical simulation is not solely from the grid convergence error, but also from many other error sources. However, one can minimise the total error by reducing the error due to grid dependence and this must be done in a systematic manner.

The purpose of this study is to assess the DNS grid convergence of flow around a square cylinder. While the results of grid refinement studies are generally reported, there is a need for a detailed assessment to be published to assist those involved in numerical simulation. Further, for the particular case of the square cylinder, there needs to be an objective method of determining adequate resolution of the boundary layers on the upstream face. This paper satisfies both these needs.

Two stages of grid refinement are involved in this study and the level of grid convergence for the later stage is evaluated using the Grid Convergence Index (GCI). A novel of assessing grid independence using Thwaites' method is also presented. DNS results from the grid with the lowest GCI are then compared with previously published data.

This report is organized as follows. After explaining the test case and the solution methodology, the first grid refinement study is presented and suggestions for grid improvements are made. A second grid refinement study is then described and the level of grid convergence is evaluated. Finally, conclusions are given in the last section.

MODEL DESCRIPTION

Test case

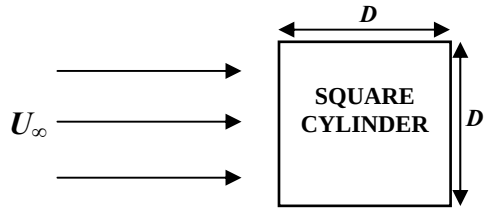

Figure 1: Schematic of flow geometry.

CASE	N_x x N_y	G_{edge}	g_u	g_d	g_{tb}	Δ_u	Δ_d	Δ_{tb}
A	625 x 230	100 x 4edges	1.0212	1.0072	1.0212	0.0592x0.01	0.01x0.045	0.01x0.0592
B	550 x 200	200 x 4edges	1.1142	1.0476	1.0985	0.0103x0.01	0.01x0.009	0.005x0.0181

Table 1: Grid parameter for case A and case B. Subscript u, d and tb represent upstream, downstream and top and bottom location respectively. The total number of nodes is N_x x N_y, number of nodes along the cylinder front edge is G_{edge}, g is cell size ratio between the adjacent cell and the cell area is Δ.

The case under investigation is a rigid square cylinder immersed in a two-dimensional uniform incompressible flow at a constant free stream velocity. Figure 1 shows a schematic illustrating the square cylinder with a side length of D, immersed in a flow with a constant free stream velocity of U_∞. The Reynolds number in this study is 150 ($Re = U_\infty D/\nu$), based on the square cylinder height D, kinematic viscosity ν and free stream velocity U_∞. All geometrical parameters and velocity flow fields are normalized by the square cylinder height D and free stream velocity U_∞ respectively.

Solution methodology

Numerical investigation by Sohankar *et al.* (1999) has shown that for Re = 150 flow around a single square cylinder, two- and three-dimensional simulations give identical results. Additionally, experimental (Luo *et al.;* 2003 and Luo *et al.*; 2007) and numerical (Saha *et al.;* 2003) studies have shown that three dimensional instability (mode A) first occurs at Re = 160. Therefore, to reduce computational cost, the flow is mathematically modelled in two-dimensional form.

The primitive variables of the flow fields are calculated numerically based on the two-dimensional unsteady incompressible Navier-Stokes and continuity equations. The OpenFOAM (Weller *et al.*; 1998) numerical simulation system is used to solve these governing equations.

The pressure implicit split operator (PISO) solution algorithm (Barton; 1998) with two correction steps for pressure-velocity coupling are used to solve these transient problems. The convergence criterion for pressure and velocity solutions are set so the residual falls below the tolerance of 10^{-6} and 10^{-5} respectively at each time step. A rectilinear grid system is applied for all cases.

In the first stage of the grid refinement study, the 1st-order implicit Euler method is used for temporal discretisation, the convection and viscous terms are discretised using the 2nd-order unbounded Gauss linear differencing scheme (central differencing). The time step for pressure, convection and diffusion terms is set at $\Delta t U_\infty/D$ = 0.005 with the requirement to keep the CFL number below 0.5.

For second stage of the grid refinement study, the temporal discretisation is advanced using a 2nd-order backward scheme. The convection term is discretised using a 2nd-order upwind scheme and for the viscous term, a 2nd-order unbounded Gauss linear differencing scheme is used. Three different time steps have been imposed corresponding to the three different grid cases so the CFL number is always less than 0.5.

GRID REFINEMENT STAGE 1

The first stage of the grid refinement is investigated by comparing the results from two DNS simulations whose only differences are the cell size and the grid stretching ratio. The case with the coarser grid is called case A and the finer one is called case B (Table 1).

Small cells are distributed near the square cylinder wall. The grid is then stretched from the first cell located at the square cylinder wall to the last cell located at along the boundary of the computational domain by adopting the following equation;

$$g = G^{1/(N-1)} \tag{1}$$

where g is cell size ratio between adjacent cells, G is the cell size ratio between the largest and the smallest cell and N is number of cells. Exception is made for the grid distribution behind the square cylinder as the wake formation length is located at around one diameter downstream from the trailing edge of the cylinder (Zdravkovich; 1987). Therefore, the grid is made uniform until two diameters downstream from the downstream edge of the cylinder before it is also stretched towards the boundary outlet. Table 1 summarizes the grid parameters for case A and case B and Figure 2 shows the cell distribution around the square cylinder for case A (top) and case B (bottom) respectively.

Flow visualisation

In the first stage of the grid refinement study, flow visualisations of each case were compared. The vorticity contour should shows a periodic staggered arrangement vortices trail behind the cylinder which is known as a von Kármán vortex street.

Figure 3 shows the instantaneous spanwise vorticity contours for case A (top) and case B (bottom). In both cases, similar vortex shedding is observed, where the free shear layers from the top and bottom sides of the cylinder roll-up downstream of the cylinder. The roll-up continues and then staggered eddies are shed downstream.

However, there are two obvious discrepancies in the vorticity distributions. First, at the square cylinder leading edges, case A has a small scattered vortices. Meanwhile for case B, the vortex smoothly sheds away from the leading edge. The second discrepancy is in the wake at a few diameters downstream from the cylinder. For case A, the wake shows a staggered arrangement of vortices with concentrated, well defined vortices of alternating sign extending downstream. For case B, the well-defined vortex structures are lost. Additionally, both cases have small spots of vorticity in the wake with case B having more spots than case A.

These observations can be related to the cell size. Case A has a coarser grid around the leading sharp edges of the square cylinder when compared with the grid of case B. From the previous study of Sohankar *et al.* (1997) the leading sharp edges are the points where the boundary layer starts to separate and the flow field gradients are high at these points. The vortex spots generated at the upstream sharp edges of the case A are believed due to the

large cell size. Then the simulation is unable to accurately resolve the high velocity gradient at the leading edges.

A similar reason can be used for the loss of well-defined vortex structures in case B. The high grading ratio (g_{tb}= 1.0985) used to stretch the grid in a transverse direction in case B created a large discrepancy in size between adjacent cells. Thus, case B had large cells only a few diameters away from the cylinder. This type of mesh produces high numerical dissipation when compared with the cell grid size used in case A.

A) Case A

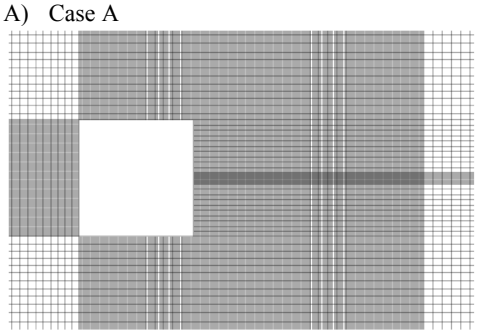

B) Case B

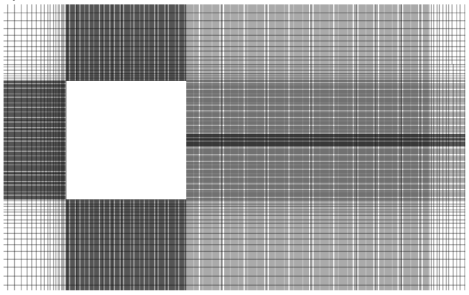

Figure 2: Cell distribution around the square cylinder.

A) Case A

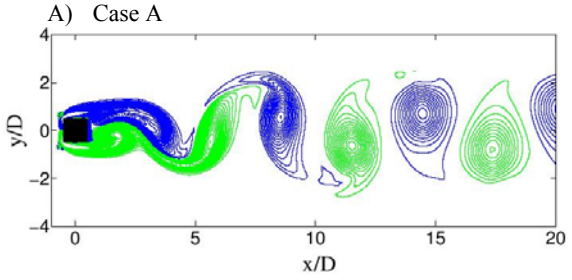

B) Case B

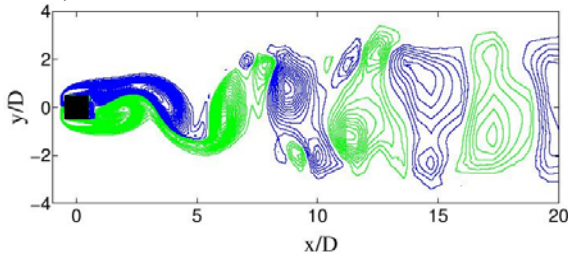

Figure 3: Instantaneous streamwise vorticity contours colored by rotation direction (blue: clockwise and green: anticlockwise), 40 equally spaced over the range -4≤ΩD/U$_\infty$≤4 (Ω is spanwise vorticity).

GRID REFINEMENT STAGE 2

In the second stage of the grid refinement study, three different grid resolutions are used. Case C has the coarsest resolution, case D has medium resolution and case E has the finest grid. Each of the grids has four zones. Extending one diameter from the cylinder wall is region (1). In this region, the cell size is uniform and is the overall minimum. From one to three diameters from the cylinder wall is region (2). The cell distribution in this region is non-uniform with the cells being stretched slowly away from the cylinder. Region (3) extends from three to ten diameters from the cylinder wall. The cells in this region were stretched and the cell size is larger than the previous two regions. From ten diameters downstream of the cylinder to the outlet of the computational domain is region (4). This region is constructed to minimize the grid stretching ratio along the wake.

The upstream, top and bottom of the boundary computational domain are 10 diameters away from the body and the outlet is 20 diameters downstream from the body. This computational domain size is similar as in simulation works by Doolan (2009) and larger than in simulation works by Sohankar *et al.* (1999).

Boundary layer thickness prediction

When fluid flows past a bluff body, boundary layers develop from each side of the stagnation point where their characteristics length scale can be very small. The characteristics of the boundary layer play an important role to the overall flow structure (i.e. flow separation), therefore it is necessary to accurately capture the boundary layer profile. This can be achieved by first evaluating the boundary layer thickness based on Thwaites' method (Thwaites; 1949).

An empirical relation for the momentum thickness (θ) based on Thwaites integral solution for incompressible laminar flow with a stagnation point on the body is;

$$\left(\frac{\theta}{L}\right)^2 R_L = \frac{0.45\upsilon}{u_e^6}\int_0^L u_e^5 ds \qquad (2)$$

where R_L is defined as $U_\infty L/\upsilon$ and υ is kinematic viscosity. The edge velocity, u_e is calculated numerically using potential flow solution and using OpenFOAM's potential flow solver to solve the equation. The integration in eqn. (2) is carried out from the stagnation point (y=0) to the front sharp corner of the square cylinder (y=L). Then, the momentum thickness is transformed into the displacement thickness using the following relationship;

$$\delta^* = \theta H(\lambda) \qquad (3)$$

where $H(\lambda)$ is a shape factor. (Refer to Cebeci and Bradshaw (1977) for the complete equation.) For laminar flow, the following approximation for the boundary layer thickness can be made;

$$\delta \approx 3\delta^* \qquad (4)$$

Figure 4 shows the comparison of boundary layer thickness (δ/D) from Thwaites' method and simulation results of case A and case B. All three lines exhibited a similar boundary layer thickness distribution. For the

simulation results (case A and case B), the boundary layer thickness is larger than the calculated value using Thwaites's method.

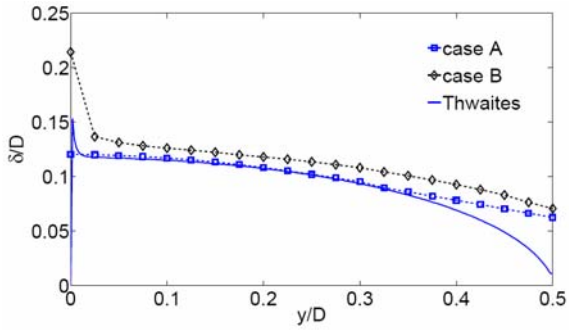

Figure 4: Boundary layer thicknesses from Thwaites' method and cases A and B.

Ideally, the smallest cell size should be considerably less than the minimum boundary layer thickness. However, as the smallest thickness of the boundary layer from Thwaites' method is nearly zero, it is difficult to achieve this. Additionally, potential flow theory does not able to accurately predict the rotational flow at the sharp corner. The true boundary layer thickness in this region is much larger as indicated by the simulations. Therefore, to make a practical grid, the cell size is based on the boundary layer thickness at position 10% before the sharp corner. From Thwaites' method calculation, the boundary layer thickness is approximately δ/D = 0.045 at that location, y/D = 0.45 from the stagnation point.

Using this approximate minimum boundary layer thickness, three different grids were constructed. The coarsest grid has approximately one cell within the boundary layer at that point, the medium grid has three and the finest one has five cells. Table 2 summarizes parameters used for case C, D and E. For each case, the grid stretching ratio in the successive regions is set as $g_{(1)} \le g_{(2)} \le g_{(3)}$ so the cells are only allowed to stretch slowly away from the cylinder.

CASE	C	D	E
N_x x N_y	259 x 252	400 x 300	520 x 440
G_{edge}	36 x 4edges	60 x 4edges	100 x 4edges
$\Delta_u = \Delta_d = \Delta_{tb}$	0.0278x0.0278	0.0167x0.0167	0.01x0.01
$g_{(1)}$	1	1	1
$g_{(2)}$	1.047	1.033	1.042
$g_{(3)}$	1.047	1.057	1.057
$\Delta t U_\infty/D$	0.002	0.005	0.005

Table 2: Grid parameter for case C, D and case E. Subscript u, d and tb represent upstream, downstream and top and bottom location respectively and subcript (1), (2) and (3) represent region 1, 2 and 3 of computational domain respectively. The total number of nodes is N_x x N_y, number of nodes along the cylinder front edge is G_{edge}, g is cell size ratio between the adjacent cell and the cell area is Δ.

The influence of the outlet boundary condition

A comparative study is carried out between two common types of computational outlet conditions. The conventional outlet boundary condition is defined as a fixed pressure value and zero streamwise velocity gradient. The second type of outlet is known as convective boundary condition. This was proposed by Orlanski (1976) for a problem of flow with a wavy structure. The following equation is used:

$$\frac{\partial U_i}{\partial t} + U_c \frac{\partial U_i}{\partial x_i} = 0 \qquad (5)$$

where indices i = 1, 2 refer to the streamwise (x) and crosswise (y) directions, respectively and U_c is the convective velocity. Following (Le et al.; 1997), the value is set to $U_c = 0.8U_\infty$.

A DNS similar to case C is carried out and it is labelled as case F. For case C, constant pressure and zero velocity gradient are applied at the outlet, meanwhile for case F, a convective boundary condition is introduced. Other parameters are kept unchanged. Both cases exhibited similar vortex shedding patterns and the vortices pass the outlet boundary smoothly. Inspection of the global results (CL_{rms}, CD_{mean}, and St) shows that both type of outlet boundary condition produced identical results.

The influence of temporal discretisation schemes

Two temporal discretisation schemes are compared to investigate the influence of higher order accuracy on the DNS results. Case D uses a 2nd-order backward Euler scheme for temporal discretisation. A second case labelled as case G uses a 1st-order Euler implicit method in time. Other parameters are keep identical between the two cases.

CASE	CL_{rms}	CD_{mean}	St
case D	0.2917	1.484	0.1577
case G	0.2849	1.478	0.1556

Table 3: Comparison of global results between DNS with 2nd-order accurate (case D) and 1st-order accurate (case G) temporal discretisation.

Inspections of the global results in Table 3 shows that the higher order scheme does not heavily influence the DNS results. Using a 1st-order scheme only slightly under predicts the global results when compared with the 2nd-order temporal scheme.

Grid convergence study using Richardson extrapolation

Richardson extrapolation (Richardson et al.: 1927) is used to calculate a higher-order estimate of the flow fields from a series of lower-order discrete values (f_1, f_2, ..., f_n). For the case of grid refinement study, the value estimated from the Richardson extrapolation is the value that would results if the cell grid size tended to zero, ($h \to 0$). The extrapolation is made from the results of at least two different grid solutions. A convergence study requires a minimum of three grid solutions (Stern et al.: 2001).

Roache (1994) generalized Richardson extrapolation by introducing the p^{th}-order methods;

$$f_{exact} \approx f_1 + \left[(f_1 - f_2)/(r^p - 1) \right] \qquad (6)$$

In this study, the grid refinement ratio r, is constant;

$$r = \Delta_C / \Delta_D = \Delta_D / \Delta_E = 1.667 \quad (7)$$

From equation (6), the extrapolated value is varied by different choice the order p. According to Stern et al. (2001) the order-of-accuracy can be estimated by using the following equation;

$$p = \frac{\ln(\varepsilon_{32} / \varepsilon_{21})}{\ln(r)} \quad (8)$$

$$\varepsilon_{i+1,i} = f_{i+1} - f_i \quad (9)$$

To evaluate the extrapolated value from these solutions, the convergence conditions of the system must be first determined. The possible convergence conditions are;

1. Monotonic convergence; $0<R<1$
2. Oscillatory convergence; $R<0$
3. Divergence; $R>1$

where R is the convergence ratio and it is determined by the equation;

$$R = \frac{\varepsilon_{21}}{\varepsilon_{32}} \quad (10)$$

Table 4 summarizes the order of accuracy for root mean square lift coefficient (CL_{rms}) and mean drag coefficient (CD_{mean}) from the simulation results on three grids. All means and root mean square results were obtained once a statistically stationary flow was observered. The convergence condition for CL_{rms} and CD_{mean} are monotonic. Strouhal number (St) is not included in this analysis as the differences between the successive grid solutions are very small (St = 0.1556, 0.1577 and 0.1602 for case C, D and E respectively). Hence, this parameter is not suitable for use in this grid refinement study.

The Grid Convergence Index (GCI) provides a uniform measure of convergence for grid refinement studies (Roache:1994). It is based on estimated fractional error derived from the generalization of Richardson extrapolation. The GCI value represents the resolution level and how much the solution approaches the asymptotic value. The GCI for the fine grid solution can be written as;

$$GCI_{i+1,i} = F_s \frac{|\varepsilon_{i+1,i}|}{f_i(r^p - 1)} \quad (11)$$

Following Wilcox (2006), the safety factor (F_s) selected for this study is 1.25.

	ε_{32} (10^{-2})	ε_{21} (10^{-2})	R	p	GCI_{32} (%)	GCI_{21} (%)
CL_{rms}	1.53	0.64	0.4183	1.7062	4.71	2.02
CD_{mean}	2.30	1.0	0.4348	1.6305	1.49	0.65

Table 4: Order of accuracy and Grid Convergence Index for three integration variables. Subscripts 3, 2 and 1 represent case C, D and E, respectively.

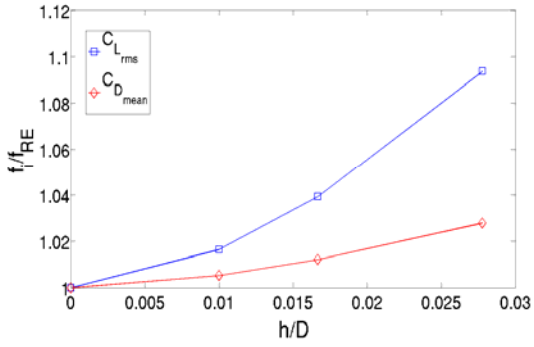

Figure 5: Comparison of global results normalized by the extrapolated value, between three grid solutions and Richardson Extrapolation estimation.
CL_{rms}; --□-- and CD_{mean}; --◊--

As listed in Table 4, there is a reduction GCI value for the successive grid refinements ($GCI_{21} < GCI_{32}$) about each of the three variables. The GCI for finer grid (GCI_{21}) is relatively low if compared to the coarser grid (GCI_{32}), indicating that the dependency of the numerical simulation on the cell size has been reduced. Additionally, as the GCI reduction from the coarser grid to the finer grid is relatively high, the grid independent solution can be said to have been nearly achieved. Further refinement of the grid will not give much change in the simulation results.

For variable CL_{rms}, the extrapolated value is only slightly lower than the finer grid solution ($h/D = 0.01$) and it is in the range of the finer grid GCI as shown in figure 5. Similar behavior is observed for variable of mean drag coefficient. Therefore, it is shown that the solution has converged with the refinement from the coarser grid to the finer grid.

Similar behavior is observed for the point variable of boundary layer thickness (δ/D). The boundary layer thickness is calculated at the leading edge of the square cylinder. As the grid is refined, the discrepancy between the solution and the extrapolated value become small. In this paper, the discrepancy between the simulation value and this extrapolated value is used to define the error,

$$E_i = \frac{f_i - f_{RE}}{f_{RE}} \quad (12)$$

Table 5 shows that the convergence condition is monotonic. The order-of-accuracy is then calculated by using equation (8) and (9) using the L^2-Norm of the values. Figure 6 shows that the successive grid refinements nearly achieved the asymptotic value at the finest grid resolution, where the relative error compared with the RE is only E_1 = 0.28%. This indicates that the boundary layer has been adequately resolved.

Variable	$\|\varepsilon_{32}/f_1\|$	$\|\varepsilon_{21}/f_2\|$	$<R>$	p	GCI_{32}	GCI_{21}
δ	0.0050	0.0172	0.275	2,(2.54)	1.21%	0.35%

Table 5: Order of accuracy and Grid Convergence Index for point variable. Subscripts 3, 2 and 1 represent case C, D and E respectively. The order of accuracy p for both variables are taken as 2 as the calculated values (indicated in a brace) exceeded the order of accuracy of the discretisation scheme.

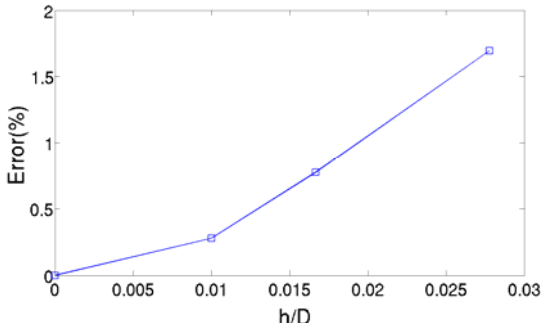

Figure 6: Percent of RMS error for boundary layer thickness along the leading edge. The order-of- accuracy, $p = 2$ and $E_1 = 0.28\%$, $E_2 = 0.77\%$ and $E_3 = 1.70\%$.

The grid convergence index (GCI) is estimated by using equation (11) with a safety factor of Fs = 1.25. As listed in the same table (Table 5), successive grid refinements resulted in a GCI reduction. Therefore, that can be said that the solution on the finest grid resolution is nearly grid independent.

Comparison of numerical data from case E with previous studies

Table 6 compares the current DNS results of case E with the summarized previous available data taken from Doolan (2009). The Strouhal number and root mean square lift coefficient from case E are in excellent agreement and in the range of the previous available data. Mean drag coefficient is slightly higher than previous studies, but is still in good agreement.

	CL_{rms}	CD_{mean}	St
Experiments (Okijama:1982, Sohankar et al.:1999)	-	1.40	0.148 to 0.155
DNS(Doolan;2009)	0.296	1.44	0.156
DNS (Sohankar et al.;1998)	0.230	1.44	0.165
DNS (Inoue et al.:2006)	0.40(peak)	1.40	0.151
current DNS (case E)	0.285	1.47	0.160

Table 6: Comparison of current DNS (case E) with previous studies listed by Doolan (2009).

III. CONCLUSION

For the first grid refinement study, flow visualization of vorticity contours from the two different grid resolutions exhibited similar behavior of some vortex spots a few diameters downstream from the square cylinder. Additionally, for case A there was a small scattered vortex near the upstream corner of the square cylinder. These observations indicated that it was necessary to refine the grid in these regions and the grid stretching ratio between cells should be minimized.

In the second grid refinement study, inspection of GCI values for integration and points variables shows that there was a gradual reduction when the grid system was refined. Comparison between the extrapolated value calculated from Richardson extrapolation indicated that the finer grid (case E) was appropriate to be used in further DNS analysis as the GCIs for all variables being studied were less than 5%.

REFERENCES

BARTON, I. E. (1998). " Comparison of SIMPLE- and PISO- type algorithms for transient flows." *International Journal for Numerical Methods in Fluids*, **26**,459-483.

CEBECI T. and BRADSHAW P. (1977). Momentum Transfer in Boundary Layers. McGraw-Hill Inc.,US.

DOOLAN, C. J. (2009). "Flat-plate interaction with the near wake of a square cylinder." *AIAA Journal*, **47**,475-478.

INOUE, O., IWAKAMI, W., and HATAKEYAMA, N. (2006). "Aeolian tones radiated from flow past two square cylinders in a side-by-side arrangement." *Physics of Fluids*, **18**(4),046104.

LE, H., MOIN, P., and KIM, J. (1997). "Direct numerical simulation of turbulent flow over a backward-facing step." *Journal of Fluid Mechanics*, **330,**349-374.

LUO, S. C., CHEW, Y. T., and NG, Y. T. (2003). "Characteristics of square cylinder wake transition flows." *Physics of Fluids*, **15**(9),2549-2559.

LUO, S. C., TONG, X. H., and KHOO, B. C. (2007). "Transition phenomena in the wake of a square cylinder." *Journal of Fluids and Structures*, **23**(2),227-248.

ORLANSKI, I. (1976). "A simple boundary condition for unbounded hyperbolic flows." *Computational Physics*, **21**(3),251-269.

OZGOREN M. (2005). " Flow structure in the downstream of a square and circular cylinders." *Flow Measurement and Instrumentation*, **17**,225-235

RICHARDSON, L. F. and GAUNT, J. A. (1927). "The deferred approach to the limit. Part I. Single lattice. Part II. Interpenetrating lattices." *Philosophical Transactions of the Royal Society of London. Series A, Containing Papers of a Mathematical or Physical Character*, **226,**299-361.

ROACHE, P. J. (1994). "Perspective: A method for uniform reporting of grid refinement studies." *Journal of Fluids Engineering*, **116**(3),405-41

SAHA, A. K., BISWAS, G. and MURALIDHAR, K. (2002). " Three-dimensional study of flow past a square cylinder at low Reynolds numbers." *International Journal of Heat and Fluid Flow*, **24**,54-66.

SOHANKAR, A., NORBERG, C., and DAVIDSON, L. (1997). "Numerical simulation of unsteady low-reynolds number flow around rectangular cylinders at incidence." *Journal of Wind Engineering and Industrial Aerodynamics*, **69-71,**189-201.

SOHANKAR, A., NORBERG, C., and DAVIDSON, L. (1998). "Low-Reynolds-number flow around a square cylinder at incidence: study of blockage, onset of vortex shedding and outlet boundary condition." *International Journal of Numerical Methods in Fluids*, **26**(1),39-56.

SOHANKAR, A., NORBERG, C., and DAVIDSON, L. (1999). "Simulation of three-dimensional flow around a square cylinder at moderate reynolds numbers." *Physics of Fluids*, **11**(2),288-306.

STERN, F., WILSON, R. V., COLEMAN, H. W., and Paterson, E. G. (2001). "Comprehensive approach to verication and validation of cfd simulations part 1: Methodology and procedures." *Journal of Fluids Engineering*, **123**(4),793-802.

THWAITES, B. (1949) "Approximate calculation of the laminar boundary layer" *Aeronautical Quarterly*, **1**,245-280.

WELLER, H. G., TABOR, G., JASAK, H., and Fureby, C. (1998). "A tensorial approach to computational continum mechanics using object-oriented techniques." *Computers in Physics,* **12,**620-631.

WILCOX, D.C. (2006), Turbulence Modeling for CFD, 3rd Ed., DCW Industries, Inc..

ZDRAVKOVICH, M. M. (1987). "The effects of interference between circular cylinders in cross flow." *Journal of Fluids and Structures*, **1**(2),239-261.